Chinese Chemical Letters 36 (2025) 110354

Contents lists available at ScienceDirect

Chinese Chemical Letters

journal homepage: www.elsevier.com/locate/cclet

Synthesis and photophysical properties of alternating donor-acceptor conjugated nanorings

Shuqi Chen[a], Cankun Zhang[b], Xiaonuo Dong[a], Hui-Jun Zhang[a], Jianbin Lin[a,*]

[a] Department of Chemistry, College of Chemistry and Chemical Engineering, The MOE Key Laboratory of Spectrochemical Analysis and Instrumentation, Xiamen University, Xiamen 361005, China
[b] Innovation Laboratory for Sciences and Technologies of Energy Materials of Fujian Province (IKKEM), Xiamen University, Xiamen 361005, China

ARTICLE INFO

Article history:
Received 23 May 2024
Revised 8 August 2024
Accepted 21 August 2024
Available online 23 August 2024

Keywords:
Nanorings
Donor-acceptor
Intramolecular charge transfer
Femtosecond transient absorption

ABSTRACT

Herein, we report the design and synthesis of alternating donor-acceptor nanorings **[3]C-NA** and **[4]C-NA**, along with a reference linear molecule **[3]L-NA**, *via* electrochemical oxidation-induced reductive elimination of alkynyl platinum(II) complexes. Unlike **[3]L-NA**, which exhibits charge defects at its end-groups, the cyclic structures of **[3]C-NA** and **[4]C-NA** facilitate enhanced electron delocalization, enabling efficient charge transfer in low-polarity toluene. In the polar solvent dichloromethane (DCM), the increased flexibility of **[4]C-NA** promotes intramolecular charge transfer and suppresses charge recombination. The observed faster intramolecular charge transfer and slower charge recombination rates in these nanoring acceptor materials suggest their potential for improving the power conversion efficiency of organic solar cells, providing valuable insights for the design of nanoring acceptor materials.

π-Conjugated macrocycles, especially those with strained π-systems, possess equivalent sites in the symmetrical cyclic structure and exhibit restricted conformational flexibility, making them ideal candidates for optoelectronic materials [1–7]. In a previous report, Colin Nuckolls and colleagues investigated the impact of structural flexibility of nanorings on the performance of devices, revealing that the less rigid nanorings have higher reorganisation energies, which in turn lead to a superior charge transport capability [8]. Therefore, establishing a connection between structural flexibility and excited-state dynamics on ultrafast time scales of these nanorings is of paramount importance.

In the realm of π-conjugated chain design, steric hindrance often leads to the formation of substantial dihedral angles between aromatic rings that are directly linked by single bonds, thereby attenuating the effectiveness of π-conjugation [9]. In contrast, the strategic incorporation of alkyne bridges, particularly butadiyne, serves to mitigate this spatial strain and promotes the adoption of a coplanar orientation among adjacent aromatic units [10,11]. Moreover, the increasing conformational flexibility found with increasing nanoring size in butadiyne-linked nanorings [12,13].

In this paper, we use dimers of 1,4-diethynylbenzene (D-DEB) as the donor unit and naphthalene diimide (NDI) as the acceptor unit [14] to construct alternating donor-acceptor molecules [15,16], referred to circular NDI-containing alkyne molecules **[3]C-NA**, **[4]C-NA** and a reference linear NDI-containing alkyne molecule **[3]L-NA** (Fig. 1). Furthermore, we investigate the effect of the structural flexibility of this series of molecules on the intramolecular charge transfer properties to provide insights for building efficient nanoring acceptor materials [17].

Because of the low stability and high reactivity of angle-strained alkynes, the synthesis of alkyne nanorings presents an exceptionally formidable challenge [11]. In the previously reported methods, the key step is to construct less-strained macrocycle precursors using *syn*-conformation corner units and then achieve alkyne nanorings by sequential bromination and elimination [18] or reduction aromatization [19–21]. Herein, we propose a strategy to construct radial π-conjugated alkyne nanorings and the synthesis procedure for NDI-based alkyne nanorings **[3]C-NA** and **[4]C-NA** is summarized in Fig. 2. The key building block is the linear terminal alkyne **1**, which can react with $PtCl_2(L_2)$ (L_2 = dppp or dppf) to obtain triangular platinum complexes **2a/b** and square platinum complexes **3a/b** [22]. In order to achieve reductive elimination of $Pt(L_2)$ from platinum complexes, we treated **2a/b** with different chemical oxidants (I_2, $AgBF_4$, XeF_2, and $NOBF_4$) [23,24] but ultimately proved unable to obtain the target nanoring **[3]C-NA**. Then, inspired by the previous work of our group [25,26], constant potential electrolysis was used to achieve reduction elimination of platinum complexes. Electrochemical oxidation-induced reduction elimination of **2b** and **3b** could be achieved by pass-

* Corresponding author.
E-mail address: jb.lin@xmu.edu.cn (J. Lin).

https://doi.org/10.1016/j.cclet.2024.110354
1001-8417/

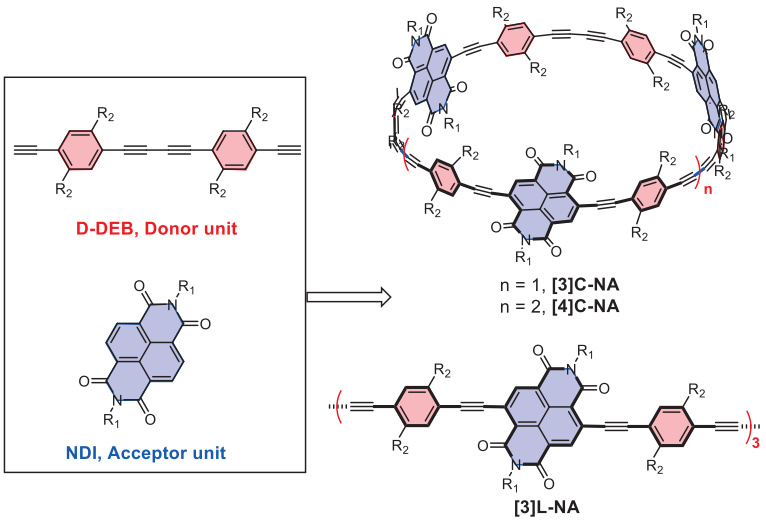

Fig. 1. Structural design of alternating donor-acceptor nanorings **[3]C-NA**, **[4]C-NA** and a linear molecule **[3]L-NA**.

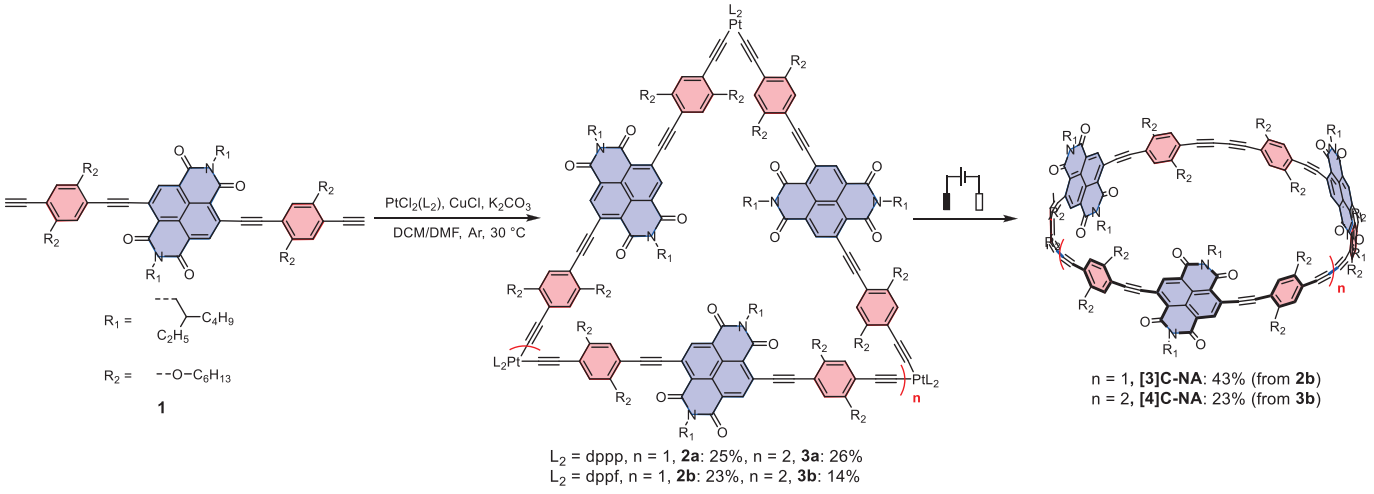

Fig. 2. Synthetics procedure toward **[3]C-NA** and **[4]C-NA**.

ing a constant potential (1.2 or 1.3 V *vs.* Ag/AgCl, Fig. S2 in Supporting information) through their DCM solutions containing electrolyte ($^{n}Bu_4NPF_6$), which gave **[3]C-NA** as a purple solid in a 43% yield and **[4]C-NA** as a dark blue solid in a 23% yield, respectively. The size of nanorings is closely related to their ring strain, which in turn significantly influences the structure and properties of the cyclic molecules. To better study the structure and properties of the alkyne nanorings, we further synthesized a reference ternary linear molecule **[3]L-NA** (see Supporting information).

The successful synthesis of **[3]C-NA**, **[4]C-NA** and **[3]L-NA** can be confirmed by NMR spectra (Fig. 3) and high-resolution MALDI-TOF mass spectra (Figs. S3–S5 in Supporting information). In the ^{1}H NMR spectra, there are only three aromatic proton signals, which reflect the highly symmetrical structures of **[3]C-NA** and **[4]C-NA** (Figs. 3a and b). In contrast, **[3]L-NA** exhibits non-equivalent aromatic proton signals due to its linear structure (Fig. 3c). And the absence of ring strain leads to rapid structural disturbance of **[3]L-NA**, resulting in very sharp proton peaks. It is worth noting that, compared to nanoring **[3]C-NA**, the ^{1}H NMR spectrum of nanoring **[4]C-NA** exhibit significant broadening. The sharp peaks of **[3]C-NA** at room temperature indicate the presence of rigid structure, and the broad peaks of **[4]C-NA** at room temperature are attributed to slow exchange that proceeds at a rate similar to the NMR time scale [27]. Subsequently, the solution-phase structure of **[4]C-NA** was investigated by variable-temperature NMR analyses (Fig. S6 in Supporting information) to reveal the difference in structural flexibility for the two nanorings. As the temperature increases, the peaks of **[4]C-NA** gradually become sharp,

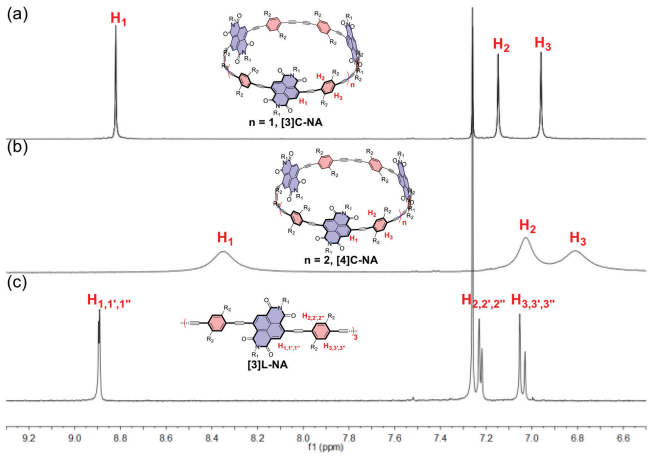

Fig. 3. Part of ^{1}H NMR spectra (298 K) of (a) **[3]C-NA**, (b) **[4]C-NA** and (c) **[3]L-NA**.

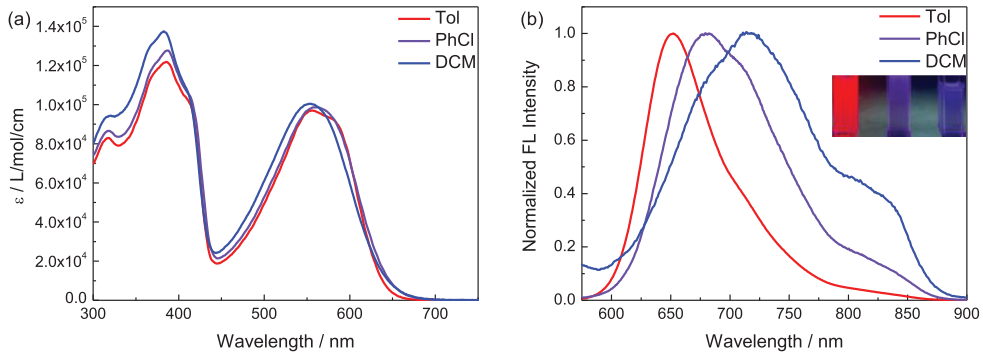

Fig. 4. Photophysical properties of **[3]C-NA** (298 K). (a) UV−vis absorption spectra and (b) fluorescence spectra of **[3]C-NA** in Tol (red), PhCl (violet) and DCM (blue). Inset: Photographs showing the fluorescence for **[3]C-NA** in Tol, PhCl and DCM under a UV lamp at $\lambda = 365$ nm.

which is generated by a time-averaged structure through rapid exchange. Conversely, at low temperature, the conformational exchange rate of **[4]C-NA** becomes slower than the NMR time scale, resulting in the coexistence of multiple conformations in the NMR spectra. Thus, the order of structural flexibility for these three molecules is **[3]C-NA** < **[4]C-NA** < **[3]L-NA**.

The photophysical properties of these three molecules were studied in solvents with varying polarity by UV-vis absorption spectroscopy and fluorescence spectroscopy. The absorption spectra of **[3]C-NA** (Fig. 4a) exhibit two absorption peaks at around 380 and 560 nm with similar molar absorption coefficients in different diluted solutions, which show not significant dependence on the polarity of solvent. However, upon careful observation of the absorption onsets in the **[3]C-NA** solution, a slight bathochromic shift was observed as the solvent polarity increased. In consideration of a large molar absorption coefficient value (*ca.* 1×10^5 L mol^{-1} cm^{-1}) of the absorption peak at around 560 nm, while donor unit **D-DEB** and acceptor unit **NDI** have no corresponding absorption peak in the region of 450–700 nm (Fig. S7 in Supporting information), the electronic transition observed at around 560 nm could be attributed to the mixed character of intramolecular charge-transfer (ICT) [16,28] and π-π^* transition.

It is noteworthy that these donor-acceptor molecules exhibit distinct ICT absorption peaks in low-polarity toluene. The nanoring **[3]C-NA** shows a maximum absorption peak at 555 nm and a red-shifted shoulder peak at 582 nm (Fig. 4a), corresponding to the (LUMO+1)←HOMO and LUMO←HOMO transitions, respectively [29]. For **[3]C-NA**, the absorbance ratio of these transitions ($A_{(\mathrm{LUMO+1)\leftarrow HOMO}}/A_{(\mathrm{LUMO\leftarrow HOMO)}}$) is 1.05. The nanoring **[4]C-NA** (Fig. S9a in Supporting information) and the reference linear molecule **[3]L-NA** (Fig. S9c in Supporting information) both display a maximum absorption peak at 582 nm along with a blue-shifted shoulder peak at 555 nm. The absorbance ratios for **[4]C-NA** and **[3]L-NA** decrease sequentially, being 0.94 and 0.85, respectively. The reduction in the ($A_{(\mathrm{LUMO+1)\leftarrow HOMO}}/A_{(\mathrm{LUMO\leftarrow HOMO)}}$) ratio indicates an increase in molecular structural flexibility.

In contrast, solvent polarity has a significant effect on fluorescence characters and the solvatofluorochromism was observed in solutions of these alternating donor-acceptor molecules (Fig. 4b). Even in a low polarity solvent Tol, **[3]C-NA** showed a low fluorescence quantum yield (Table 1, $\lambda_{em} = 652$ nm, $\varphi_f = 1.83\%$). And in a solution with higher polarity, such as DCM, **[3]C-NA** is virtually non-fluorescent (Table 1, $\lambda_{em} = 712$ nm, $\varphi_f = 0.16\%$), revealing strong ICT character in the excited states of this nanoring. Obviously, the higher the polarity of the solvent, the more pronounced the red-shift of the fluorescence emission peak. Fig. S8 shows the wavenumber against the solvent parameter $E_T(30)$ fits to a linear line that undoubtedly indicating the positive solvatofluorochromic effect of **[3]C-NA** [30–33].

Table 1
The summary of photophysical properties.

Compound	Absorption max. (nm)			Fluorescence max. (nm)			φ_f (%)		
	Tol	PhCl	DCM	Tol	PhCl	DCM	Tol	PhCl	DCM
[3]C-NA	555	560	555	652	683	712	1.83	0.18	0.16
[4]C-NA	582	576	565	648	678	722	1.93	0.24	0.16
[3]L-NA	582	577	567	637	668	714	2.87	0.38	0.20

Similarly, **[4]C-NA** and **[3]L-NA** exhibit intramolecular charge transfer and positive solvatofluorochromism (Figs. S9 and S10 in Supporting information). In addition, the linear molecule **[3]L-NA** shows the largest emission redshift (**[3]C-NA**: $\Delta\nu = 1371$ cm^{-1}; **[4]C-NA**: $\Delta\nu = 1582$ cm^{-1}; **[3]L-NA**: $\Delta\nu = 1694$ cm^{-1}), indicating greater structural flexibility in its excited state, which dissipates energy through thermal processes due to the free rotation of the donor and acceptor units [34,35]. The relevant photophysical data for nanorings **[3]C-NA**, **[4]C-NA**, and a linear molecule **[3]L-NA** are summarized in Table 1. In contrast to cycloparaphenylenes (CPPs), whose absorption maxima exhibit negligible changes upon increasing nanoring size [9], the absorption maxima of ***[n]*C-NA** demonstrate red shifts with increasing conjugation length. In low-polarity toluene, the emission maxima show no significant size-dependency. However, in dichloromethane (DCM), the emission maxima shift to longer wavelengths with increasing nanoring repetitive units. The photophysical study reveals that donor-acceptor nanorings exhibit size-dependent properties distinct from CPPs, suggesting their potential as a novel class of optoelectronic materials.

Femtosecond transient absorption (fs-TA) measurements were further devoted to unravel the connection between molecular structure and charge transfer. At a low polarity solvent Tol, the fs-TA spectra of nanoring **[3]C-NA** show the negative ground-state bleach (GSB) in the range of 550–620 nm and the positive excited singlet state absorption (ESA) in the range of 620–950 nm after photoexcitation at the initial time (Fig. S12a in Supporting information). Subsequently, the GSB signal at 580 nm and the ESA signal at 740 nm decay gradually, by a concomitant growth of a new species appears near 630 nm. According to the radical anion/cation control experiments (Fig. S11 in Supporting information) and the reported spectral positions of NDI radicals [36], the formation of new band can be attributed to the NDI radical anion and the D-DEB radical cation, confirming the generation of charge transfer state (CT) [37]. Because of the gradual growth of CT states in **[3]C-NA**, the influence of vibrational relaxation should be taken into account during dynamics analysis, thus requiring three exponents to achieve the best fitting (Fig. S12b in Supporting information). The

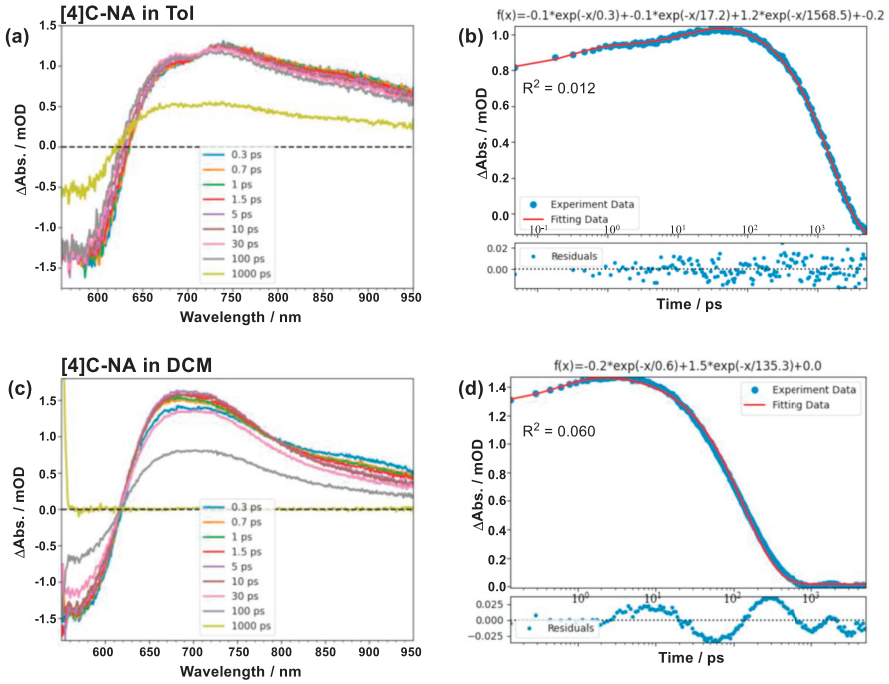

Fig. 5. The fs-TA spectra of **[4]C-NA** (298 K) in (a) Tol and (c) DCM following the excitation at 550 nm, and the dynamics traces superimposed with fitted curves at (b) 670 nm in Tol and (d) 660 nm in DCM.

first time constant of rigid nanoring **[3]C-NA** in Tol corresponds to vibrational relaxation ($\tau_{VR} = 3.7$ ps), followed by intramolecular charge transfer and charge recombination with the time constants of $\tau_{CT} = 22.3$ ps and $\tau_{CR} = 1637.4$ ps, respectively. For nanoring **[4]C-NA** with enhanced structural flexibility, its excited singlet states can achieve rapid vibrational relaxation accompanied by intramolecular charge transfer. Apparently, the fs-TA show the coexistence of ESA signal at 740 nm and CT state signal at 670 nm after photoexcitation at the initial time (Fig. 5a), but the dynamic processes of these two signals are different. The ESA signal attenuates with the increase of time, while the signal in the CT state increases first and then decreases (Fig. S14b in Supporting information). The fitting results of the nanoring **[4]C-NA** show that the first relaxation process with time constant of about 0.3 ps, which is attributed to the rapid vibrational relaxation. The time constants of subsequent charge transfer and charge recombination are $\tau_{CT} = 17.2$ ps and $\tau_{CR} = 1568.5$ ps, respectively (Fig. 5b). However, the fs-TA spectra of **[3]L-NA** are significantly distinct. The decay of ESA signal near 720 nm is not accompanied by a corresponding growth of CT state signal at low wavelength (Fig. S13a in Supporting information), but the ESA band undergoes a blue shift upon photoexcitation, which is indicative of energy dissipation through vibrational relaxation. Thus, the excited state of **[3]L-NA** consists of only two dynamical processes (Fig. S13b in Supporting information). The first time constant corresponds to the vibration relaxation $\tau_{VR} = 12.0$ ps, and the second time constant is attributed to the decay of the excited singlet state ($\tau_{S1} = 1871.8$ ps). There is a pronounced divergence in the excited state dynamics between nanorings and linear molecules when observed in low polarity Tol. This is because the terminal groups of linear molecules are chemically distinct from the internal molecular environment, resulting in charge defects that are not conducive to efficient charge transfer and charge carrier transport. In contrast, nanorings have a highly symmetrical structure that facilitates better charge delocalization.

In polar DCM, the fs-TA spectra of **[3]C-NA**, **[4]C-NA** and **[3]L-NA** similarly display a positive band at around 660 nm and a pronounced negative band at around 570 nm (Fig. 5c, Figs. S12c and S13c in Supporting information). For these three molecules, by comparing the fs-TA spectra with the radical anion/cation control experiments (Fig. S11 in Supporting information), it can be determined that the CT band (at 660 nm) is generated upon photoexcitation. Despite a considerable spectral overlap between the ESA signal and the CT state signal, the temporal dynamics of these signals reveal distinct behaviors. The trend chart, as depicted in Figs. S14d–f (Supporting information), shows that over time, the signal intensity at 900 nm monotone decreasing, while the signal at 660 nm exhibits an initial increase followed by a subsequent decline. This pattern of signal evolution provides further evidence for the occurrence of a charge transfer process within the system. The spectral alterations observed for nanoring **[4]C-NA** during the initial 1.5 ps are less pronounced than those of **[3]C-NA** and **[3]L-NA** (Fig. 5c, Figs. S12c and S13c), which can be attributed to the presence of faster charge transfer dynamics in **[4]C-NA**. In polar solvents, since vibrational relaxation and charge transfer occur almost simultaneously, only two exponents are required for dynamics fitting. According to the fitting results, the charge transfer and charge recombination time constants of nanoring **[3]C-NA** in DCM are $\tau_{CT} = 0.9$ ps and $\tau_{CR} = 37.8$ ps, respectively (Fig. S12d in Supporting information). For the linear molecule **[3]L-NA** in DCM, the charge transfer and charge recombination time constants are $\tau_{CT} = 0.9$ ps and $\tau_{CR} = 36.7$ ps, respectively (Fig. S13d in Supporting information). In contrast, flexible nanoring **[4]C-NA** have a faster charge transfer rate and a slower charge recombination rate in DCM, which are $\tau_{CT} = 0.6$ ps and $\tau_{CR} = 135.3$ ps, respectively (Fig. 5d). The rate constant ratio for **[4]C-NA**, $k_{CT}/k_{CR} = \tau_{CR}/\tau_{CT} = 226$, is 5.4 times that of the rigid nanoring **[3]C-NA**, which has a ratio of $k_{CT}/k_{CR} = \tau_{CR}/\tau_{CT} = 42$. This observation can be attributed to the enhanced structural flexibility of **[4]C-NA** compared to the rigid nanoring **[3]C-NA**. The capac-

ity of **[4]C-NA** to adopt a twisted three-dimensional conformation is instrumental in promoting more efficient intramolecular charge transfer. Moreover, this structural characteristic also contributes to the suppression of charge recombination processes, thereby favouring the overall charge dynamics within the system. An accelerated rate of intramolecular charge transfer coupled with a decelerated rate of charge recombination in the acceptor materials is advantageous for enhancing the energy conversion efficiency of organic solar cells. Among them, the structural flexibility of the cyclic acceptor is the key to the design of the acceptor materials.

In summary, we successfully synthesize nanorings **[3]C-NA**, **[4]C-NA** as well as a linear molecule **[3]L-NA** and revealed the difference of molecular structural flexibility: **[3]C-NA** < **[4]C-NA** < **[3]L-NA**. These molecules possess an alternating donor-acceptor structure, exhibiting distinct intramolecular charge transfer and solvatofluorochromism. The results of excited-state dynamics indicate that the linear molecule **[3]L-NA**, which has the greatest structural flexibility, is limited by the charge defects produced by its end-groups and does not exhibit superior charge transfer properties compared to the cyclic molecules. In contrast, the nanorings **[3]C-NA** and **[4]C-NA** support better charge delocalization and undergo intramolecular charge transfer in a low polarity solvent like Tol. The structural flexibility of nanorings has a significant impact on their charge transfer properties. In polar DCM solution, compared to the rigid nanoring **[3]C-NA**, the structurally perturbed nanoring **[4]C-NA** adopts a twisted three-dimensional structure that facilitates accelerated intramolecular charge transfer and slowed charge recombination, revealing its potential as an acceptor material for organic solar cells. This research presents a viable strategy for the design and synthesis of alkyne nanorings and emphasizes the important influence of the structural flexibility of nanorings on the photophysical properties, which has a guiding significance for understanding the structure-property relationship of the nanorings and expanding its applications in optoelectronic devices.

Declaration of competing interest

The authors declare that there are no conflicts of interest to disclose in relation to this manuscript. All financial and personal relationships that could influence the results or interpretation of this work have been disclosed. The research was conducted independently and without any influence from external sources.

CRediT authorship contribution statement

Shuqi Chen: Data curation. **Cankun Zhang:** Data curation. **Xiaonuo Dong:** Data curation. **Hui-Jun Zhang:** Formal analysis. **Jianbin Lin:** Writing – review & editing, Supervision, Conceptualization.

Acknowledgments

We thank the financial support from Natural Science Foundation of China (Nos. 22271239, 22171237, 22071208, and 92356308), and the Natural Science Foundation of Fujian Province (2022J01524).

Supplementary materials

Supplementary material associated with this article can be found, in the online version, at doi:10.1016/j.cclet.2024.110354.

References

[1] B. Zhang, R. Hernández Sánchez, Y. Zhong, et al., Nat. Commun. 9 (2018) 1957.
[2] M. Ball, B. Zhang, Y. Zhong, et al., Acc. Chem. Res. 52 (2019) 1068–1078.
[3] E.J. Leonhardt, R. Jasti, Nat. Rev. Chem. 3 (2019) 672–686.
[4] Y. Li, H. Kono, T. Maekawa, et al., Acc. Mater. Res. 2 (2021) 681–691.
[5] H. Cong, Y. Luan, Synlett 28 (2017) 1383–1388.
[6] S. Zhong, L. Zhu, S. Wu, et al., Chin. Chem. Lett. 34 (2023) 108124.
[7] H. Zhang, J. Lin, Chin. J. Org. Chem. 42 (2022) 3437–3455.
[8] M.L. Ball, B. Zhang, Q. Xu, et al., J. Am. Chem. Soc. 140 (2018) 10135–10139.
[9] E.R. Darzi, R. Jasti, Chem. Soc. Rev. 44 (2015) 6401–6410.
[10] M. Rickhaus, A. Vargas Jentzsch, L. Tejerina, et al., J. Am. Chem. Soc. 139 (2017) 16502–16505.
[11] K. Miki, K. Ohe, Chem. Eur. J. 26 (12) (2019) 2529–2575.
[12] A. Vyšniauskas, M. Qurashi, N. Gallop, et al., Chem. Sci. 6 (2015) 5773–5778.
[13] P. Liu, Y. Hisamune, M.D. Peeks, et al., Angew. Chem. Int. Ed. 55 (2016) 8358–8362.
[14] A. Nowak-Król, K. Shoyama, M. Stolte, et al., Chem. Commun. 54 (2018) 13763–13772.
[15] Q. Wu, D. Deng, K. Lu, et al., Chin. Chem. Lett. 28 (2017) 2065–2077.
[16] D. Jia, H. Zhong, S. Jiang, et al., Chin. Chem. Lett. 33 (2022) 4900–4903.
[17] M. Ball, Y. Zhong, B. Fowler, et al., J. Am. Chem. Soc. 138 (2016) 12861–12867.
[18] T. Kawase, H.R. Darabi, M. Oda, Angew. Chem. Int. Ed. 35 (1996) 2664–2666.
[19] K. Miki, T. Matsushita, Y. Inoue, et al., Chem. Commun. 49 (2013) 9092–9094.
[20] S. Lee, E. Chénard, D.L. Gray, et al., J. Am. Chem. Soc. 138 (2016) 13814–13817.
[21] T.A. Schaub, J.T. Margraf, L. Zakharov, et al., Angew. Chem. Int. Ed. 57 (2018) 16348–16353.
[22] L. Zhao, B.H. Northrop, P. Stang, J J, Am. Chem. Soc. 130 (2008) 11886–11888.
[23] G. Fuhrmann, T. Debaerdemaeker, P. Bäuerle, Chem. Commun. 38 (2003) 948–949.
[24] E. Kayahara, T. Iwamoto, T. Suzuki, et al., Chem. Lett. 42 (2013) 621–623.
[25] L. Zhang, G. Zhang, H. Qu, et al., Angew. Chem. Int. Ed. 60 (2021) 24543–24548.
[26] F. Su, Y. Hong, G. Zhang, et al., Chem. Sci. 15 (2024) 5604–5611.
[27] Z. Sun, T. Suenaga, P. Sarkar, et al., Proc. Natl. Acad. Sci. U. S. A. 113 (2016) 8109–8114.
[28] Y. Wang, Z. He, G. Chen, et al., Chin. Chem. Lett. 28 (2017) 2133–2138.
[29] S.K. Keshri, A. Takai, T. Ishizuka, et al., Angew. Chem. Int. Ed. 59 (2020) 5254–5258.
[30] C. Reichardt, Chem. Rev. 94 (1994) 2319–2358.
[31] T. Kuwabara, J. Orii, Y. Segawa, et al., Angew. Chem. Int. Ed. 54 (2015) 9646–9649.
[32] S. Nishigaki, M. Fukui, H. Sugiyama, et al., Chem. Eur. J. 23 (2017) 7227–7231.
[33] X. Chen, J. Hu, J. Lin, et al., Chin. Chem. Lett. 36 (2025) 109923.
[34] Z. Kuang, G. He, H. Song, et al., J. Phys. Chem. C 122 (2018) 3727–3737.
[35] S. Izumi, H.F. Higginbotham, A. Nyga, et al., J. Am. Chem. Soc. 142 (2020) 1482–1491.
[36] S. Gámez-Valenzuela, I. Torres-Moya, A. Sánchez, et al., Chem. Eur. J. 29 (2023) e202301639.
[37] J. Jiang, A. Alsam, S. Wang, et al., J. Phys. Chem. A 121 (2017) 4891–4901.